Optimal Control of a Magnetic Bearing without Bias Flux Using Finite Voltage

Charles Yang *, Research Assistant
Carl Knospe, Associate Professor
Panagiotis Tsiotras, Assistant Professor
Department of Mechanical and Aerospace Engineering
University of Virginia, Charlottesville, VA 22903

charles.yang@alliedsignal.com, crk4y@virginia.edu, tsiotras@virginia.edu

* currently with AlliedSignal Automotive SRS7000 19 Mile RD, Sterling Heights, MI 48314

SUMMARY

Conventional Active Magnetic Bearings (AMB) are operated using a bias current (or flux) to achieve greater linearity and dynamic capability. Bias, however, results in undesirable rotating losses and consequent rotor heating. While control without bias flux is an attractive alternative, it is considerably more complex due to both force slew rate limitations and actuator nonlinearity. In this paper, optimal control of a magnetic bearing without bias is investigated. A single degree-of-freedom system consisting of a mass and two opposing electromagnets is considered. The optimal control problem is examined for a cost function that penalizes both poor regulation and rotational energy lost. Though a standard optimization procedure does not directly yield an analytical solution, it does show that the optimal control is always bang-bang including possibly a singular arc. First, the minimum time problem is solved for a simple switching law in three dimensional state space. A non-standard, physics-based approach is then employed to obtain an optimal solution for the general problem. The final result is an optimal variable structure feedback controller. This result provides a benchmark which can be used for evaluation of the performance of a practical feedback controller designed via other methods. The practical controller will be designed to support a flexible rotor and achieve robustness and optimally reject disturbance. This result may also be applied to many other applications which contain opposing quadratic actuators.

KEY WORDS: active magnetic bearing; opposing quadratic actuators; nonlinear; constrained control; time-state optimization; bang-bang; singular arc.

1. INTRODUCTION

1.1. Active magnetic bearings

An active magnetic bearing (AMB) uses attractive forces generated by electromagnets to support a rotating shaft. This noncontacting bearing offers many advantages and opportunities for a wide variety of industrial, medical, and scientific applications. A standard AMB is composed of electromagnetic actuators, sensors, a controller, and power amplifiers. A rotor position signal, measured by a sensor, is processed by a controller to generate appropriate signals for the power amplifiers that deliver current to each of the actuator coils. This feedback control results in stable suspension of the rotor. Switching amplifiers are commonly used, and their power supply has a finite voltage. This limitation on amplifier voltage has important implications for the achievable AMB force slew rate (i.e., time derivative of force). A common approach to improve the force slew rate is to introduce a bias current (or flux ϕ). With a bias, the actuator may also be accurately modeled as linear. The disadvantage of operation with a bias is the associated ohmic loss in the coil ($IR^2 \propto \phi^2$), rotating hysteresis loss ($\propto \phi$), alternating hysteresis loss ($\propto \phi^{1.6}$), and eddy current loss ($\propto \phi^2$) [1]. For high speed rotating machinery, the eddy current loss is dominant; herein we refer to it as the rotating loss. This rotating loss may result in excessive rotor heating. Moreover, it results in decreased machine efficiency. Thus, operation without bias is appealing in applications where efficiency is critical, for example energy storage flywheels.

The problem considered herein is much more general than the AMB application context given. It concerns the issue of controlling opposing quadratic actuators without preload. This problem and the control difficulties due to its force slew rate limitations can be found in many fields.

1.2. Previous research

Since an AMB system is highly nonlinear without bias, researchers have investigated nonlinear control techniques to achieve stability and performance. Levine, et al. proposed a nonlinear control of AMB based on exact feedback linearization techniques which may require unbounded control (voltage) unless suitable reference trajectory is prescribed [2]. Charara, et al. studied sliding mode control using I/O linearization of AMB, but this was not based on minimization of a cost function [3]. Furthermore, the control effort with this method may be very large. Though a nonlinear fuzzy controller for AMB proposed by Weidemann and Xiao dealt with constrained control, numerical methods are needed to design an optimal fuzzy controller [4]. It appears that literature does not contain a solution to the optimal nonlinear control of AMB with bounded voltage. Published research on time-optimal control of linear third order systems with control constraints, Pao and Franklin [5], Kalman [6], is similar to that reported here. However, these efforts do not consider the combined minimum time-state problem which has a considerably more complex solution due to singular trajectories.

1.3. Overview of the paper

The contents of the paper are as follows. The advantages of bias and the difficulties encountered without it are examined in section 2. In section 3, the system dynamics model is developed in state space form. Section 4 is devoted to the analysis of the optimal control problem without bias flux. A minimum time problem is solved in section 5 which yields a simple analytical solution. In section 6, a solution to the optimal problem is obtained in a non-standard, physics-based approach. Section 7 geometrically describes optimal trajectories in the three dimensional state space and derives a variable structure control law. In section 8, we numerically verify the solution found in section 6. The last section contains a short conclusion and discussion of future work.

2. OPERATION WITH AND WITHOUT BIAS

Conventional AMBs typically employ a bias current (or flux) to achieve greater linearity and dynamic capability. To illustrate this, consider the simple system consisting of two opposing electromagnets shown in Figure 1.

Figure 1. Opposing magnets

The net force generated by the opposing magnets is

$$f = \frac{\mu_o N^2 A_g}{4}\left(\frac{i_1^2}{(g_o - x)^2} - \frac{i_2^2}{(g_o + x)^2}\right) \tag{1}$$

All variables are defined in Appendix I.

2.1. Advantages of bias

As indicated in equation (1), the force is a quadratic function of the currents i_1 and i_2. If these two currents are operated as perturbations i_p about a bias I_b

$$\begin{aligned} i_1 &= I_b + i_p \\ i_2 &= I_b - i_p \end{aligned} \tag{2}$$

then the force is exactly linear in the perturbation current when the displacement x is zero

$$f = \left(\frac{\mu_o N^2 A_g I_b}{g_o^2}\right) i_p \tag{3}$$

With small displacements, the force may be expressed via a linearized Taylor's series expansion of equation (1) as

$$f \cong \left(\frac{\mu_o N^2 A_g I_b}{g_o^2}\right) i_p + \left(-\frac{\mu_o N^2 A_g I_b^2}{g_o^3}\right) x \tag{4}$$

This linear approximation for the force is usually quite adequate and greatly simplifies the design of feedback controllers.

Another motivation for bias operation is the achievable force slew rate. For example, in the case of zero displacement, the maximum rate of change of force is bounded by

$$\left|\frac{df}{dt}\right| \le c\left|\frac{di_p}{dt}\right|_{\max} \tag{5}$$

where $c = \dfrac{\mu_o N^2 A_g I_b}{g_o^2}$

Furthermore, the rate of change of the current is bounded by

$$\left|\frac{di_p}{dt}\right| \le \frac{V_{\max}}{L} \tag{6}$$

where the actuator inductance L is given by

$$L = \frac{N^2 A_g \mu_o}{2g} \tag{7}$$

From equations (5), (6), and (7) a bound on the achievable force slew rate for an AMB with bias current I_b is

$$\left|\frac{df}{dt}\right| \le \frac{2 I_b V_{\max}}{g_o} \tag{8}$$

Thus, the bias current value directly determines the achievable force slew rate. With reasonable amplifier voltage, a wide range of force signals can be produced. For these reasons, operation about a bias has been widely used in AMB applications.

2.2 Operation without Bias

If a bias is not employed, then only one of the opposing electromagnets is exerting a force at any time. Here and throughout the remainder of this papers we will formulate the equations in terms of flux for simplicity but without loss of generality. The force produced by each of the electromagnets in Figure 1 is given by the expression.

$$f_j = \frac{\phi_j^2}{A_g \mu_o}, \qquad j = 1,2 \tag{9}$$

where ϕ_j is the magnetic flux which is a function of the current i and air gap g, $\phi_j = \dfrac{A_g \mu_o N i_j}{2 g_j}$.

The bound on force slew rate is then

$$\left|\frac{df_j}{dt}\right| \le \frac{2}{A_g \mu_o}\left|\phi_j\right|\left|\dot{\phi}_j\right| \tag{10}$$

The governing equations of the electrical system then yield the following bound on the rate of change of flux.

$$\left|\dot{\phi}_j\right| \le \frac{V_{\max}}{N} \tag{11}$$

Equations (9), (10), (11) together yield

$$\left|\frac{df_j}{dt}\right| \le \frac{2V_{\max}}{N\sqrt{\mu_o A_g}}\sqrt{\left|f_j\right|} \tag{12}$$

Equation (12) indicates that the achievable force slew rate at any time is a function of the currently applied force. When the applied force is zero, the force slew rate is also zero. This is in contrast to the case of operation with bias where the slew rate limitation is independent of the currently applied force, equation (8). This constraint on achievable force has a profound impact on the issue of control. To examine this, the optimal control without bias flux of the simple system illustrated in Figure 1 will be studied.

3. SYSTEM DYNAMICS

Since only one electromagnet is active at a time, a single new flux variable ϕ for the two electromagnet system shown in Figure 1 may be defined as

$$\phi = \begin{cases} \phi_1 & \phi_1 > 0,\ \phi_2 = 0 \\ 0 & \phi_1 = 0,\ \phi_2 = 0 \\ -\phi_2 & \phi_1 = 0,\ \phi_2 > 0 \end{cases}$$

The force f then can be expressed as

$$f = |\phi|\phi$$

and

$$\dot{\phi} = u$$

where u is the amplifier power supply voltage.
Using the following states

$$x_1 = x$$
$$x_2 = \dot{x}_1$$
$$x_3 = \phi$$

the dynamic model of the system is described by the equations

$$\begin{aligned} \dot{x}_1 &= x_2 \\ \dot{x}_2 &= |x_3|x_3 \\ \dot{x}_3 &= u \end{aligned} \tag{13}$$

where appropriate units have been chosen to simplify the equations.

Without loss of generality, we will set the power supply voltage such that the control (amplifier voltage) is limited by $|u| \le 1$. The system dynamics are shown in block diagram form in Figure 2.

Figure 2. System block diagram

This system is nonlinear and has a constraint on control effort. Linearization of the system equations about the origin yields an uncontrollable system. Furthermore, the control constraint prevents successful application of input-output feedback linearization since this yields unbounded control in general. Thus, the fundamental problems of control cannot be ameliorated via conventional linear approaches.

4. OPTIMAL CONTROL

4.1. Cost function

The control objective is to drive the position, velocity, and flux to zero from an arbitrary initial condition in finite time, that is

$$x(T_0) = x_0, \qquad x(T_f) = 0 \tag{14}$$

It is desirable to do this regulation without excessive rotating and ohmic losses. Since these losses are proportional to ϕ^2, the cost function has been chosen as

$$J = \alpha T_f + (1-\alpha)\int_{T_0}^{T_f} x_3^2 dt \tag{15}$$

where α is the relative weighting. Equation (15) will be referred to as the time-loss cost function.

This cost function represents a tradeoff between regulation speed (authority) and rotational energy lost during the regulation period. Consider two extreme cases:

i. If there is no penalty on time, $\alpha = 0$, then the optimal control will produce a (perhaps infinitely short) flux pulse that gives the mass an infinitesimal velocity towards the origin. The mass then coasts to the origin over infinite time with no flux applied. Obviously, the regulation time is infinite for this case but the integral of flux squared is minimal.

ii. If the regulation time is critical ($\alpha = 1$), then the optimal control will be the minimum time solution. This case is the same as the Mayer problem where the integral term is dropped, Bryson and Ho [7].

4.2. Optimization

Following the standard optimization procedure, the Hamiltonian *H* is obtained as

$$H = \lambda^T f + L = \lambda_1 x_2 + \lambda_2 |x_3| x_3 + \lambda_3 u + (1-\alpha) x_3^2 \tag{16}$$

Because *H* is not an explicit function of time, *H* must be constant. The transversality condition yields

$$H = H(T_f) = \alpha \tag{17}$$

The Euler-Lagrange condition, $\dot{\lambda}^T = -H_x$, yields

$$\begin{aligned} \dot{\lambda}_1 &= 0 \\ \dot{\lambda}_2 &= -\lambda_1 \\ \dot{\lambda}_3 &= -(2\lambda_2 |x_3| + 2(1-\alpha) x_3) \end{aligned} \tag{18}$$

which can be integrated to provide

$$\begin{aligned} \lambda_1 &= c_1 \\ \lambda_2 &= -c_1 t + c_2 \\ \dot{\lambda}_3 &= -2\left[(-c_1 t + c_2)|x_3| + (1-\alpha) x_3\right] \end{aligned} \tag{19}$$

And the optimality condition yields

$$\frac{\partial H}{\partial u} = \lambda_3 = 0$$

Unfortunately, this condition does not yield an explicit optimal control. However, according to Pontryagin's minimum principle

$$H(x^*, u^*, \lambda^*) \le H(x^*, u, \lambda^*)$$

where * represents the optimal, i.e., an optimal control must minimize the Hamiltonian. Therefore, to minimize the Hamiltonian (16), with control constraint

$$|u| \le 1$$

the control law is then given by

$$u = -\operatorname{sgn}(\lambda_3) \tag{20}$$

where the switching function is given by

$$\lambda_3 = -2\int_0^t \left((c_2 - c_1 t)|x_3| + (1-\alpha) x_3\right) dt + \lambda_3(0)$$

A singular arc may also be part of the optimal trajectory. The standard method for checking the existence of a singular arc is to take successive time derivatives of $\frac{\partial H}{\partial u}$, and set each equal to zero, continuing until the control appears. For the problem considered, this method yields

$$\frac{d}{dt}\frac{\partial H}{\partial u} = \dot{\lambda}_3 = -\left(2\lambda_2|x_3| + 2x_3\right) = 0 \tag{21}$$

The second derivative would then yield the control (since $\dot{x}_3 = u$), however this method cannot be applied directly since $\frac{d}{dt}|x_3|$ is not defined at $x_3 = 0$ which will be a common occurrence.

Equation (21) indicates three possible solutions:

$i)\ x_3 > 0, \lambda_2 = \alpha - 1$,
$ii)\ x_3 = 0, \lambda_2 = arbitrary$,
$iii)\ x_3 < 0, \lambda_2 = 1 - \alpha$.

Assume that solution i) is true over all or a portion of the singular arc, that is $x_3 > 0$ and $\lambda_2 = \alpha - 1$. Since $\lambda_2 = \alpha - 1$ is assumed to be true over this portion of the singular arc, $\dot{\lambda}_2 = 0$. However, from equation (19) this implies that $\lambda_1 = 0$. Therefore, the co-states in this case are $\lambda_1 = 0$, $\lambda_2 = \alpha - 1$, $\lambda_3 = 0$. Substitution of these values into the Hamiltonian yields $H = 0$. From equation (17), however, $H = \alpha$. This contradiction excludes case i) from the singular arc condition. A similar procedure can also show the same contradiction for case iii). Therefore, the only case to satisfy equation (21) is case $ii)\ x_3 = 0,\ \lambda_2 = arbitrary$. This condition must hold over the singular arc, hence $\dot{x}_3 = 0$. The singular control, therefore, is $u = \dot{x}_3 = 0$. For the singular control to be part of an optimal trajectory, the "convex condition"

$$(-1)^k \frac{\partial}{\partial u}\left[\left(\frac{d}{dt}\right)^{2k} \frac{\partial H}{\partial u}\right] \geq 0 \tag{22}$$

must also be satisfied. Here, $k = \frac{n}{2} - 1$, where n is the number of derivatives that control u appears (details see Bryson & Ho [7]). This condition cannot be evaluated for this case since $\frac{d}{dt}|x_3|$ is not defined at $x_3 = 0$. Although the optimality may be proved rigorously using nonsmooth analysis methods such as Clarke's generalized gradients [8], the authors chose to take advantage of the physical knowledge of the system and use numerical methods to verify instead. An example case is given in section 8.

To summarize, the optimal control solution to the time-loss problem is then characterized by equation (20) with possibly a singular arc (dependent on the initial condition).

4.3. Discussion of optimal control

For an arbitrary initial condition, it is impossible to directly find an analytic solution for the optimal control since the switching function λ_3 cannot be evaluated. Numerical solution is possible but difficult using methods such as the multiple shooting algorithm and dynamic programming, Stoer and Bulirsch [9], Jacobson and Mayne [10]. However, this yields little insight into the problem. Thus, it will only be used to verify the analytical results, which is discussed in section 6.

The problem may be solved, however, by taking advantage of the important characteristics of the optimal control solution found above, namely that the optimal control must always be composed of the segments $u = +1$, $u = -1$, and $u = 0$ when $x_3 = 0$.

5. TIME OPTIMAL CONTROL

From the analysis presented in section 4, the time-loss optimal control must always be composed of bang-bang controls: $u = +1$, $u = -1$, and possibly singular control: $u = 0$. Correspondingly, optimal trajectories are always composed of bang-bang trajectories and possibly a singular arc. It is beneficial to examine the minimum time solution to this problem. An understanding of the bang-bang solution provides valuable insight into the time-loss problem posed by equations (14) and (15). Moreover, for some initial conditions the solution to the time-loss problem contains no singular arcs, which means that the bang-bang solution is optimal. For this problem, we may construct a control law and geometrically interpret the optimal control in the x_1-x_2-x_3 state space.

5.1. Bang curve

Intuitively, trajectories from certain initial conditions can be driven to the origin with only $+1$ or -1 control. To find these unique initial conditions, the equations of motion may be integrated backwards in time from the origin with either $u = +1$ or $u = -1$ control. Figure 3 illustrates these trajectories.

Figure 3. ± Bang trajectories

Any initial condition lying on this curve can be driven to the origin with a single 'bang' of voltage in a time optimal fashion. The locus of these points will be referred to as the bang curve which can be expressed by a parametric function

$$x_1 = \pm\frac{\tau^4}{12}$$

$$x_2 = \mp\frac{\tau^3}{3}$$

$$x_3 = \pm\tau$$

where $\tau > 0$.

5.2. Bang-bang surface

Starting with points on the bang curve as initial conditions, a surface of time optimal trajectories can be generated by another backward integration in time using the opposite control. For example, for points on the $u = -1$ bang curve, the control $u = +1$ is employed in the backward integration. After some laborious but trivial algebra, the resulting surface can be described by $B = 0$ where

$$B = 27\left(4x_1 + 4\,\mathrm{sgn}(z)x_2x_3 + \mathrm{sgn}(x_3)x_3^4\right)^3 + 32\,\mathrm{sgn}(z)\left(\mathrm{sgn}(x_3)x_3^3 + 3\,\mathrm{sgn}(z)x_2\right)^4 \tag{23}$$

and

$$z = x_2 + \frac{x_3^3}{3} \tag{24}$$

Figure 4 shows some trajectories on this bang-bang surface in the three dimensional state space.

Figure 4. Bang-bang surface in three dimensional state space

This bang-bang surface is analogous to (and resembles) the classic two dimensional phase plane plot of the solution to the minimum time problem of a double integrator with control constraints. The ± Bang curve is analogous to the switching curve of the two dimensional case. The control $u = -1$ is employed on one-half of the surface, whereas $u = +1$ is used on the other half of the surface.

For later use, the curve where the bang-bang surface intersects the x_1-x_2 plane is designated as the bang-bang curve, which can be described as

$$x_1^3 + \frac{3}{2}\mathrm{sgn}(x_2)x_2^4 = 0 \tag{25}$$

5.3. Bang-bang-bang space

Analogous to the switching curve in the two dimensional problem, the bang-bang surface divides the space into two subspaces: $u = -1$ is employed for subspace above the switching surface, whereas $u = +1$ is used for subspace below. Clearly, the state can be driven from any initial condition to the origin with three or fewer voltage switches in the following manner: the first bang drives the state to the bang-bang surface, the second bang then drives the state along the surface to the bang curve, and the final bang drives the state along the bang curve to the origin. The control law may be written as

$$u = \begin{cases} -\operatorname{sgn}(B) & B \neq 0,\ z \neq 0 \\ -\operatorname{sgn}(z) & B = 0,\ z \neq 0 \\ -\operatorname{sgn}(x_3) & B = 0,\ z = 0 \end{cases} \tag{26}$$

where B and z are defined in equations (23) and (24).

5.4. Discussion of minimum time solution

The bang-bang surface of the minimum time solution divides the state space into two subspaces ($B > 0$, $B < 0$) where opposite control voltages ($u = +1$, $u = -1$) are applied to drive the state onto the bang-bang surface. Depending on the relative weighting α (e.g., $\alpha \to 1$), some trajectories on the bang-bang surface are optimal for the time-loss performance function, equation (15) as well. This insight begs the question: for what other regions of the state space will the control prescribed by the minimum time solution, equation (26), be the same as that for the time-loss solution?

Consider the optimal control for points in the subspace

$$\Pi_1 = \{(x_1, x_2, x_3) : B > 0,\ x_3 > 0\}$$

(the region above both the bang-bang surface and the x_1-x_2 plane in Figure 4). Application of the control $u = +1$ will increase both the time required for regulation (since the minimum time solution uses $u = -1$) and the losses incurred (since $x_3 > 0$ and $u = +1$ will increase x_3). Therefore, in this subspace the time-loss optimal control is the same as the minimum time optimal control. Similarly, in the subspace

$$\Pi_2 = \{(x_1, x_2, x_3) : B < 0,\ x_3 < 0\}$$

the control $u = +1$ is optimal for both the minimum time and time-loss cost functions.

The time-loss optimal control for points in the subspaces

$$\Pi_3 = \{(x_1, x_2, x_3) : B > 0,\ x_3 \leq 0\}$$

and

$$\Pi_4 = \{(x_1, x_2, x_3) : B < 0,\ x_3 \geq 0\}$$

is not as clear as that in subspaces Π_1 and Π_2. In the subspaces Π_3 and Π_4, the trade-off between regulation and losses becomes important. The control action chosen may decrease one of the terms in the cost function at the expense of the other term. In the next section we derive the time-loss optimal control in the subspace Π_3 and examine how the solution's geometry gives rise to the singular solutions.

6. OPTIMAL SOLUTION IN SUBSPACES

6.1. Optimal solution in subspace Π_3

Due to symmetry, only the subspace Π_3 is considered. For an arbitrary initial condition in this subspace, the time-loss optimal trajectory is composed of bang trajectories and possibly a singular arc. An optimal control candidate is shown in Figure 5 along with the corresponding flux

Figure 5. Optimal control candidate for subspace Π_3

where the time intervals are chosen to minimize the cost *J*. The optimality proof of this control strategy is straightforward. A control with more switches will result in the same loss (since loss is equal to magnitude of the net change in velocity) but longer regulation time (since the control trajectories through periods t_1, t_2 and t_3 are minimum time solutions for the given boundary conditions). The optimality of this control strategy is also verified via a numerical method in section 8.

Integrating the state equations from the initial conditions to the final conditions yields

$$x_2(T_f) = x_{20} - x_{30}^2 t_1 + x_{30} t_1^2 - \frac{t_1^3}{3} - \frac{t_2^3}{3} + \frac{t_3^3}{12} = 0 \tag{27}$$

$$\begin{aligned} x_1(T_f) &= \left(-\frac{2}{3}t_1^4 + \frac{8}{3}x_{30}t_1^3 - 4x_{30}^2 t_1^2 + \left(2x_{30}^3 + 2x_{20}\right)t_1 - \frac{1}{4}x_{30}^4 - x_{30}x_{20} + x_{10} \right) \\ &+ \left(x_{20} - x_{30}^2 t_1 + x_{30} t_1^2 - \frac{t_1^3}{3} - \frac{t_2^3}{3} \right)\left(t_s + t_3\right) + \frac{t_3^4}{24} = 0 \end{aligned} \tag{28}$$

and

$$x_{30} - t_1 + t_2 = 0 \tag{29}$$

the cost becomes

$$J = \alpha T_f + (1-\alpha)\int_{T_0}^{T_f} x_3^2 dt = \alpha(t_1 + t_2 + t_s + t_3) + (1-\alpha)\left(x_{30}^2 t_1 - x_{30} t_1^2 + \frac{1}{3}t_1^3 + \frac{1}{3}t_2^3 + \frac{t_3^3}{12} \right)$$

The minimum value of the cost function is found by setting

$$\frac{\partial J}{\partial t_1} = 0 \tag{30}$$

and solving for the optimal value of t_1. This method of solution for the optimal time relies upon *J* being convex in t_1, which is proved in Appendix II. For an arbitrary initial condition in subspace Π_3, the optimal solution is found by solving for the time intervals using equations (27), (28), (29) and (30), which is detailed in Appendix III.

During the time interval t_3, the state is moving along the bang-bang surface and bang curve examined in section 5. During the singular time interval t_s, the state moves in the x_1-x_2 plane since the singular control can only occur when $x_3 = 0$. The state must move through the subspace Π_3 during time intervals t_1 and t_2 and must either encounter, (1) the bang-bang surface at the end of time interval t_1 (in which case, $t_s = 0$) , or (2) a singular surface in the x_1-x_2 plane at the end time interval t_2.

To leave the subspace Π_3 via the singular surface, the switch between $u = -1$ and $u = +1$ must occur before the state reaches the bang-bang surface. The set of all points at which this switch occurs defines a switching surface that is very useful in constructing the time-loss optimal control solution in subspace Π_3.

For points on this surface, the first time interval t_1 is equal to zero. By setting $t_1 = 0$ in equation (AIV.6), the switching surface in subspace Π_3 can be described by $\{(x_1, x_2, x_3) : S = 0,\ B > 0,\ x_3 < 0\}$ where

$$S = \left(-36\alpha x_1 + (1-\alpha)72x_2^2 + 12\alpha x_2 x_3 + (1-\alpha)48x_2 x_3^3 + \alpha x_3^4 + (1-\alpha)8x_3^6\right)^3 + 32\alpha^3\left(3x_2 + x_3^3\right)^4$$

Note that state trajectories do not travel along the switching surface as they do along the bang-bang surface. The switching surface is shown in Figure 7 in section 7 for reasons of space. The control employed in subspace Π_3 is then $u = -\mathrm{sgn}(S)$. By symmetry, the switching surfaces in subspace Π_3 and Π_4 can be described by

$$S = \left(\mp 36\alpha x_1 + (1-\alpha)72x_2^2 + 12\alpha x_2 x_3 + (1-\alpha)48x_2 x_3^3 + \alpha x_3^4 + (1-\alpha)8x_3^6\right)^3 + 32\alpha^3\left(\pm 3x_2 \pm x_3^3\right)^4 \tag{31}$$

6.2. Singular surface

The curve at which the switching surface intersects the x_1-x_2 plane is a special case where $x_3 = 0$ and $t_1 = 0$. In this case, equation (29) yields $t_2 = 0$ and the singular control $u = 0$ is first applied as indicated in Figure 5. For convenience, this curve is denoted as the switching curve and can be determined by setting $x_3 = 0$ in equation (31). The switching curve is given by $y = 0$, where

$$y = \left(\mp 36\alpha x_1 + (1-\alpha)72 x_2^2\right)^3 + 32\alpha^3 (3x_2)^4 \tag{32}$$

A singular arc is part of the optimal trajectory for initial conditions in the x_1-x_2 plane between the switching and bang-bang curve as shown in Figure 6 (shaded region).

Figure 6. Singular surface

This singular surface, is the union of all possible singular arcs which are shown in the figure with arrows indicating the movement of the state in time. There are parallel to the x_1 axis since the velocity is constant during coasting. The unshaded region between the two curves is the non-physical case where $t_s < 0$. Here, the intersection point can be found by solving equations (25) and (32), which yields

$$\tilde{x}_1 = \pm \frac{1}{6}\left(\frac{\alpha}{1-\alpha}\right)^2 \tag{33a}$$

$$\tilde{x}_2 = \mp \sqrt{\frac{1}{18}\left(\frac{\alpha}{1-\alpha}\right)^3} \tag{33b}$$

As indicated in equations (33a) and (33b), the location of this intersection point is determined by the weighting factor α. Consider two extreme cases: i). As the time penalty approaches zero ($\alpha \to 0$), equations (33a) and (33b) yield $\tilde{x}_1 \to 0$ and $\tilde{x}_2 \to 0$. This implies that the switching curve collapses onto x_1 axis. The increase in the singular surface area indicates that more optimal trajectories contain a singular arc. In this case, the optimal control produces an infinitesimal velocity in the appropriate direction and a consequent infinite time to reach the origin. ii). If the regulation time is critical, $\alpha \to 1$, equations (33a) and (33b) yield $\tilde{x}_1 \to \infty$ and $\tilde{x}_2 \to \infty$, which implies that the singular surface recedes to infinity. The optimal solution, in this case, is bang-bang control as discussed in section 5.

7. OPTIMAL CONTROL SOLUTION

7.1. Optimal trajectories

Combining the results from section 5 and 6, the time-loss optimal control throughout the state space is completely described. This also produces a useful depiction of the optimal trajectories in the state space. Figure 7 shows a typical three-switch optimal trajectory with a singular arc.

Figure 7. An optimal trajectory in 3-D state space

Starting at the indicated initial condition, the control $u = -1$ drives the state through the x_1-x_2 plane to the switching surface. The control is then changed to $u = +1$ which drives the state to the singular surface in the x_1-x_2 plane. The singular control $u = 0$ is then used and the state travels along a singular arc until it reaches the bang-bang surface (bang-bang curve). Then, the state is driven to the origin in the same manner as the minimum time solution.

7.2. Optimal control law

The geometric interpretation of the control strategy presented above may be used to derive an optimal control law. This may be considered to be a variable structure feedback controller for the problem, which may be written as

$$u = \begin{cases} v & B \neq 0,\ z \neq 0 \\ -\mathrm{sgn}(z) & B = 0,\ z \neq 0 \\ -\mathrm{sgn}(x_3) & B = 0,\ z = 0 \end{cases}$$

where

$$v = \begin{cases} -\operatorname{sgn}(B) & \operatorname{sgn}(B)\operatorname{sgn}(x_3) > 0 \\ -\operatorname{sgn}(S) & \operatorname{sgn}(B)\operatorname{sgn}(x_3) < 0 \\ w & x_3 = 0 \end{cases}$$

$$w = \begin{cases} -\operatorname{sgn}(B) & \operatorname{sgn}(B)\operatorname{sgn}(x_3) > 0 \\ -\operatorname{sgn}(B) & \operatorname{sgn}(B)\operatorname{sgn}(x_3) < 0,\ |x_1| < |\tilde{x}_1| \\ 0 & \operatorname{sgn}(B)\operatorname{sgn}(x_3) < 0,\ |x_1| > |\tilde{x}_1| \end{cases}$$

where B, z, S, and $\tilde{x}_1$ are defined in equations (23), (24), (31), and (33a) respectively.

7.3. Discussion

The investigation above yields some insights to the fundamental nature of the problem. For an arbitrary initial condition, three or less switches in voltage can drive the state to the origin in minimum time. The energy loss is proportional to the velocity change in magnitude. Depending on the initial condition and the time weighting factor α, a singular arc can be part of the optimal trajectory to achieve minimum cost J. The effective switching surface and corresponding singular surface are a function of the time weighting factor α, whereas the bang-bang surface is invariant of α.

8. NUMERICAL VERIFICATION

In this section we verify numerically the optimal solution obtained in the earlier sections. We use the necessary conditions in equations (13) and (18) along with the boundary conditions (14) and the transversality condition (17) to formulate a two-point boundary value problem (TPBVP). The problem is subsequently solved using the multiple-shooting method [11] . The software BNDSCO [12] is a FORTRAN code that implements this method. It can handle very general optimal control problems involving state and control constraints, multiple switching points, etc. Multiple shooting methods, in contrast to single-shooting methods, perform integration of the trajectory over a finite number of nodes. Therefore, they require initial guesses (*both* for states and co-states) at every node. This makes them difficult to coverge in the absence of very good initial guesses. On the other hand, since the trajectory integration (particularly of the co-state system) is performed over smaller time intervals, multiple-shooting methods are, in general, numerically more robust than single-shooting methods.

To handle the issue of accurate initial guesses (which includes the correct switching structure) we used direct optimization. Specifically, the initial guesses for BNDSCO were generated using EZOPT, a direct optimization software which uses collocation and provides a gateway to NPSOL, a nonlinear optimization program, (see Gill et. al.[13] for details). Instead of *postulating* a switching structure for the optimal solution, we have used the (approximate) solution provided by EZOPT to generate the initial guesses for BNDSCO. We did not impose any switching structure a priori, although we could have done this using the analysis of sections 4-7. This allows the independent verification of the analytic results of the previous sections.

Direct optimization methods (such as the one used in EZOPT) provide the optimal trajectory and the corresponding control inputs at discrete time instances. Thus, initial guesses for the states and the corresponding switching times become readily available for the multiple-shooting method. Indirect optimization requires, however, initial guesses of the co-states as well. Initial guesses of the co-states can be determined using the methodology of Seywald and Kumar [14]. Essentially, the time history of the co-states can be calculated from the corresponding sensitivities of the cost with respect to the states. We do not delve into detail on this approach and we refer the intested reader to reference 14.

In order to avoid numerical difficulties with the non-smooth (not C^2) function $|x_3|x_3$ in (13) we approximate this function using

$$|x_3|x_3 = \operatorname{sgn}(x_3)x_3^2 \approx \frac{2}{\pi}\operatorname{atan}(\rho x_3)x_3^2 \tag{34}$$

where $\rho >> 1$. This function is infinitely differentiable and more well-behaved in the neighborhood of zero. Apart from numerical well-posedness, the approximation is also justified by the fact that, in practice, switchings are never instantaneous. Moreover, the approximation in equation (34) becomes increasingly accurate as $\rho \to \infty$. For the subsequent simulations $\rho = 10$ was used.

Using the previously described approach we have generated optimal trajectories for two cases. The first case corresponds to $\alpha = 0.7$ with initial conditions $x_1 = 1, x_2 = x_3 = 0.5$. The solution given by EZOPT (using 41 discrete nodes) is denoted by the circles in Figure 8a. The solution is bang-bang as it is evident by the control history in Figure 8b. Using these initial guesses and the corresponding co-states, BNDSCO converged within five iterations. The final solution is shown in Figure 8b. The solution is indeed optimal (better, satisfies the necessary conditions for optimality). This is evident from Figure 8b, where the history of the switching function is plotted along with the control input. In this figure, the left scale denotes the control input and the right scale denotes the switching function. The control switches when the switching function crosses zero. The optimal solution is the same as predicted by the analysis in sections 6 for these values of α and the initial conditions.

Figure 8: Numerical solution of the optimal control problem (α=0.7 case). (a) states, (b) control and switching function. The small circles denote the solution from EZOPT (41 nodes). The solid lines denote the exact solution obtained by BNDSCO.

More interesting is the bang-bang-singular-bang-bang case. The theoretical analysis in sections 6 and 7 predicts that this switching structure is optimal for $\alpha = 0.07$ and initial conditions as before. Direct optimization codes are notorious for being unable to locate singular arcs accurately. This was also evident in our problem. Figure 9a shows the solution predicted by EZOPT (denoted by the circles). The oscillatory behavior in the middle of the trajectory is an artifact of the numerical difficulty encountered by the program on the singular arc. (We have shown that the only possible optimal values for the control is 0 or $\pm$ 1.) More nodes may be introduced in the singular arc to increase the accuracy, but this may lead to more oscillatory behavior. Using the values of the states shown in Figure 9a we calculated the corresponding co-states. With these initial guesses, BNDSCO converged within eight iterations. The final solution obtained from BNDSCO is shown in Figure 9b (solid line). The optimality of the control is also verified in Figure 9b where the switching function is plotted versus time. The swicthing function is positive when u = -1, negative when u = +1 and identically zero on the singular arc (u = 0). Kelley's necessary condition[15],as well as McDanell-Powers[16] necessary conditions for joining optimal singular and nonsingular arcs were checked and were shown to be satisfied. The result of Figure 9b is the same as the one predicted from the analysis in section 6.

Figure 9: Numerical solution of the optimal control problem (α=0.07 case). (a) states, (b) control and switching function. The small circles denote the solution from EZOPT (41 nodes). The solid lines denote the exact solution obtained by BNDSCO.

8. CONCLUSION

In this paper, time-loss optimal control of AMB without bias is investigated. A mass and two opposing electromagnets model is treated as a triple integrator nonlinear system with control constraint. The optimal control problem is solved for a cost function that represents a trade-off between regulation (time) and energy loss. The solution may be interpreted as an optimal variable structure feedback controller. The analytical solution was numerically verified by solving the corresponding two-point boundary value problem using a multiple-shooting method. Initial guesses for the multiple-shooting method were generated by direct optimization. Apart from the easiness of generating initial guesses, this approach has the benefit of avoiding the postulation of an optimal switching structure. The numerical results verified the optimal switching structure found in section 7.

This controller is not practical for implementation since it concerns only a single axis, does not consider system uncertainties or disturbances, and requires full state feedback. Indeed, solution of even a simple rigid rotor problem using the methods employed herein would be extremely difficult. Nevertheless, the investigation yields valuable insights into the nature of the problem, which can be utilized in future controller design efforts. Also, it provides a benchmark for the evaluation of the performance of more practical feedback controller designed via other methods.

ACKNOWLEDGMENTS

The authors wish to thank Professor Miles Townsend for many helpful suggestions and Dr. Hans Seywald of Analytics Mechanics and Associates for providing them with a copy of EZOPT and for helpful discussions. They also thank Haijun Shen for his assistance in running BNDSCO and EZOPT.

APPENDIX I: NOMENCLATURE

i	coil current
V	amplifier voltage
L	coil inductance
N	coil turns
A_g	gap area
g_o	nominal air gap
g	air gap
x	displacement
μ_o	permeability of free space
B	magnetic flux density
ϕ	magnetic flux
I_b	bias current
i_p	perturbation current
λ	Lagrange multipliers

APPENDIX II: PROOF OF CONVEXITY OF COST J IN t_1

Following the materials in section 6.1, we wish to show that $\left.\frac{\partial^2 J}{\partial t_1^{\,2}}\right|_{t_{1,\min}} > 0$, where $t_{1,opt}$ is obtained from

$$\frac{\partial J}{\partial t_1} = 0 \tag{AIII.1}$$

Unfortunately, it is not possible to obtain an analytical expression for $t_{1,opt}$ from equation (AIII.1). However, it is possible to show J is convex in t_s, that is to show $\left.\frac{\partial^2 J}{\partial t_s^{\,2}}\right|_{t_{s,opt}} > 0$, where $t_{s,opt}$ is obtained from $\frac{\partial J}{\partial t_s} = 0$. If a one-to-one relationship between t_1 and t_s can be shown, that is to show $\frac{\partial t_1}{\partial t_s} \neq 0$, then, J must be convex in t_1.

Manipulation of equations (27), (28), and (29) yields

$$\frac{\partial t_s}{\partial t_1} = -\frac{2}{t_3^3}\left(12 t_s t_2^2 + 8 t_2^3 + 10 t_2^2 t_3 + t_3^3\right) \neq 0 \tag{AIII.2}$$

since all time intervals are greater than zero. Equation (AIII.2) also indicates that t_s decreases as t_1 increases.

The value $t_{s,opt}$ can be obtained by solving $\frac{\partial J}{\partial t_s}=0$, which gives

$$t_{s,opt}=\frac{1}{6\alpha}t_3^3-\frac{2}{3}t_2-\frac{1}{2}t_3$$

After laborious algebra, the following result may be obtained

$$\left.\frac{\partial^2 J}{\partial t_s{}^2}\right|_{t_{s,opt}}=\frac{8\alpha^2 t_2^2\left(3\alpha t_2^2+\alpha t_3^2+6t_2^2t_3^2\right)}{t_3\left(4\alpha t_2^2+\alpha t_3^2+2t_2^2t_3^2\right)^2}>0$$

Since there is a one-to-one relationship between t_1 and t_s, J is also convex in t_1. The convexity can also be shown for the other case in subspace Π_4 in a similar fashion.

APPENDIX III: OPTIMAL SOLUTION IN SUBSPACE Π_3

Following the materials in section 6.1, the cost is

$$J=\alpha\left(t_1+t_2+t_s+t_3\right)+(1-\alpha)\left(x_{30}^2t_1-x_{30}t_1^2+\frac{1}{3}t_1^3+\frac{1}{3}t_2^3+\frac{t_3^3}{12}\right) \qquad \text{(AIV.1)}$$

From equations (27), (28) and (29), we can derive the following

$$t_2=t_1-x_{30} \qquad \text{(AIV.2)}$$

$$t_3=\left(-12x_{20}+12x_{30}^2t_1-12x_{30}t_1^2+4t_1^3+4\left(t_1-x_3\right)^3\right)^{\frac{1}{3}} \qquad \text{(AIV.3)}$$

$$t_s=\left(-8t_1^4+32x_{30}t_1^3-48x_{30}^2t_1^2+12\left(2x_{30}^3+2x_{20}\right)t_1-3x_{30}^4-12x_{30}x_{20}+12x_{10}\right)t_3^{-3}-\frac{t_3}{2} \qquad \text{(AIV.4)}$$

Substitution of equation (AIV.2), (AIV.3) and (AIV.4) into equation (AIV.1) yields

$$\begin{aligned}J=&\ \alpha t_1+\alpha\left(t_1-x_{30}\right)+\alpha\left(-8t_1^4+32x_{30}t_1^3-48x_{30}^2t_1^2+12\left(2x_{30}^3+2x_{20}\right)t_1-3x_{30}^4-12x_{30}x_{20}+12x_{10}\right).\\&\left(-12x_{20}+12x_{30}^2t_1-12x_{30}t_1^2+4t_1^3+4\left(t_1-x_3\right)^3\right)+\frac{1}{2}\left(-12x_{20}+12x_{30}^2t_1-12x_{30}t_1^2+4t_1^3+4\left(t_1-x_3\right)^3\right)^{\frac{1}{3}}\\&+(1-\alpha)\left(x_{30}^2t_1-x_{30}t_1^2+\frac{1}{3}t_1^3+\frac{1}{3}\left(t_1-x_{30}\right)^3+\frac{1}{12}\left(-12x_{20}+12x_{30}^2t_1-12x_{30}t_1^2+4t_1^3+4\left(t_1-x_3\right)^3\right)\right)\end{aligned} \qquad \text{(AIV.5)}$$

which is only in terms of t_1. The optimal value of t_1 can be determined by

$$\begin{aligned}\frac{\partial J}{\partial t_1}=&\ 2\alpha+\alpha\frac{\left(-32t_1^3+96x_{30}t_1^2-96x_{30}^2t_1+12\left(2x_{30}^3+2x_{20}\right)\right)}{-12x_{20}+12x_{30}^2t_1-12x_{30}t_1^2+4t_1^3+4\left(t_1-x_{30}\right)^3}+\alpha\frac{\left(12x_{30}^2-24x_{30}t_1+12t_1^2+12\left(t_1-x_{30}\right)^2\right)}{6\left(-12x_{20}+12x_{30}^2t_1-12x_{30}t_1^2+4t_1^3+4\left(t_1-x_{30}\right)^3\right)^{\frac{2}{3}}}\\&-\alpha\frac{\left(-8t_1^4+32x_{30}t_1^3-48x_{30}^2t_1^2+12\left(2x_{30}^3+2x_{20}\right)t_1-3x_{30}^4-12x_{30}x_{20}+12x_{10}\right)\left(12x_{30}^2-24x_{30}t_1+12t_1^2+12\left(t_1-x_{30}\right)^2\right)}{\left(-12x_{20}+12x_{30}^2t_1-12x_{30}t_1^2+4t_1^3+4\left(t_1-x_{30}\right)^3\right)^2}\\&+(1-\alpha)\left(2t_1^2-4t_1x_{30}+2x_{30}^2+\frac{1}{12}\left(12x_{30}^2-24x_{30}t_1+12t_1^2+12\left(t_1-x_{30}\right)^2\right)\right)=0\end{aligned} \qquad \text{(AIV.6)}$$

REFERENCES

1. Kasarda, M. E. F., P. E. Allaire, E. H. Maslen, G. R. Brown, and G. T. Gillies, 'High speed rotor losses in a radial 8-pole magnetic bearing, part 2: analytical/empirical models and calculations', Paper 96-GT-471, *Int. Gas Turbine Conference* (1996).

2. Levine, J., J. Lottin, and J.-C. Ponsart, 'A nonlinear approach to the control of magnetic bearings', *IEEE Trans. Control Systems Tech.*, Special Issue On Magnetic Bearing Control, Vol. 4, No. 5 (1996).
3. Charara, A., J. De Miras, and B. Caron, 'Nonlinear control of a magnetic levitation system without pre-magnetization', *IEEE Trans. Control Systems Tech.*, Special Issue On Magnetic Bearing Control, Vol. 4, No. 5 (1996).
4. Weidemann, B. and W. Xiao, ‘A nonlinear fuzzy controller for magnetic bearings without premagnetization’, *In Proceedings of the Fourth International Symposium on Magnetic Bearings* (1994).
5. Pao, L. Y. and G. F. Franklin, ‘Proximate time-optimal control of third-order servomechanisms’, *IEEE Transactions on Automatic Control*, vol. 30, No. 4, 560-580 (1993).
6. Kalman, R. E., ‘Analysis and design principles of second and higher order saturating servomechanisms’, *AIEE Trans.*, vol. 74, 102-118 (1955).
7. Bryson, A. and Y. Ho, *Applied Optimal Control*, Hemisphere Publishing Corp., Bristol. PA, 1975.
8. Clarke, F., *Optimization and Nonsmooth Analysis*, John Wiley & Sons, New York, 1983.
9. Stoer, J. and R. Bulirsch, *Introduction to Numerical Analysis*, Springer, New York, 1983.
10. Jacobson, D. H. and D. Q. Mayne, *Differential Dynamic Programming*, American Elsevier, New York, 1970.
11. Burlisch, R., "Einfuhrung in die Flugbahnoptimierung die Mehrzielmethode zur Numerischen Losung von Nictlinearen Randvertproblemen und Aufgaben der Optimalen Steuerung," Lehrgang Flugbahnoptimierung, Carl-Cranz-Gesellschaft e.v., October 1971, (in german).
12. Oberle, H. J., and Grimm, W., "BNDSCO: A Program for the Numerical Solution of Optimal Control Problems," DFVLR-Mitt. 85-05, 1985 (in german).
13. Gill, P. E., Murray, W., Saunders, M. A., Wright, M. H., "User's guide for NPSOL (version 4.0). Report SOL 86-2. Dept. of Operations Research, Stanford University, CA, 1986.
14. Seywald, H. and Kumar, R. R., "Method for Automatic CoState Calculation." *AIAA Journal of Guidance, Control, and Dynamics,* Vol. 19, no. 6, 1996, pp. 1252--1261.
15. Kelley, H. J., "A Second-Variation Test for Singular Extremals," *AIAA Journal*, Vol. 2, no. 8, 1964, pp. 1380--1382.
16. McDanell, J. P. and Powers, W. F., "Necessary Conditions for Joining Optimal Singular and Nonsingular Subarcs," *SIAM Journal on Control*, Vol. 9, no. 2, 1971, pp. 161-173.

Figure 1

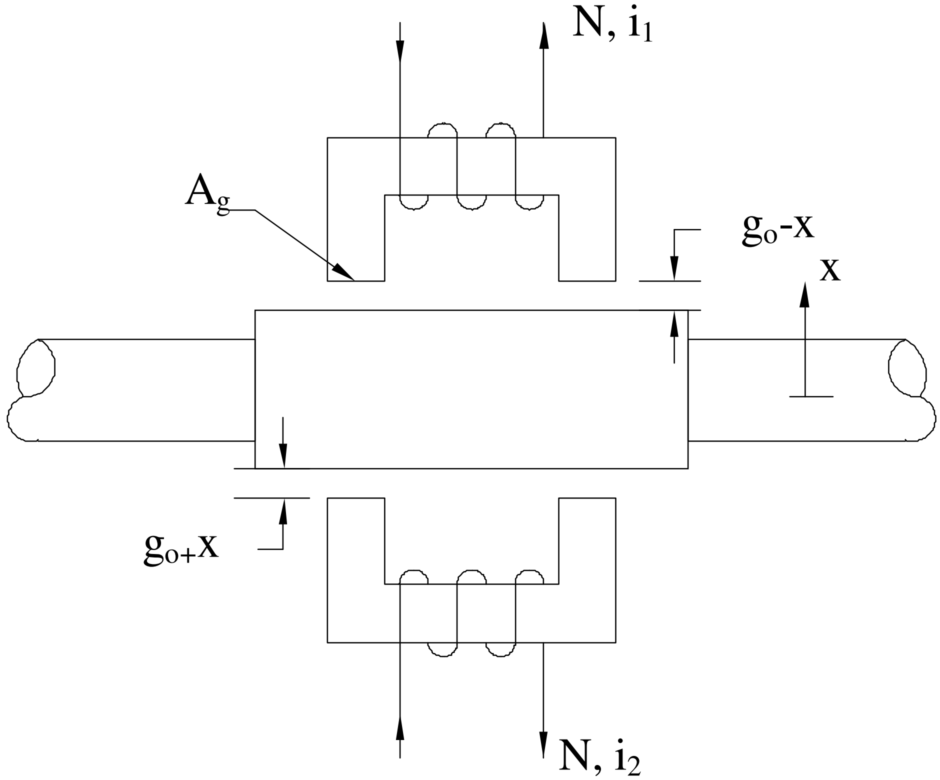

Figure 2

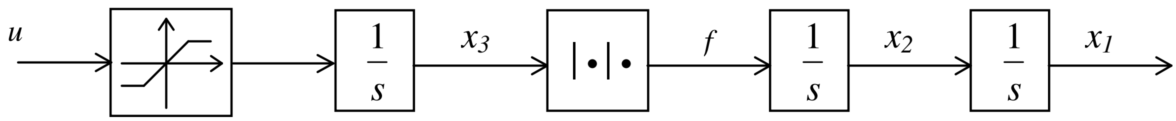

Figure 3

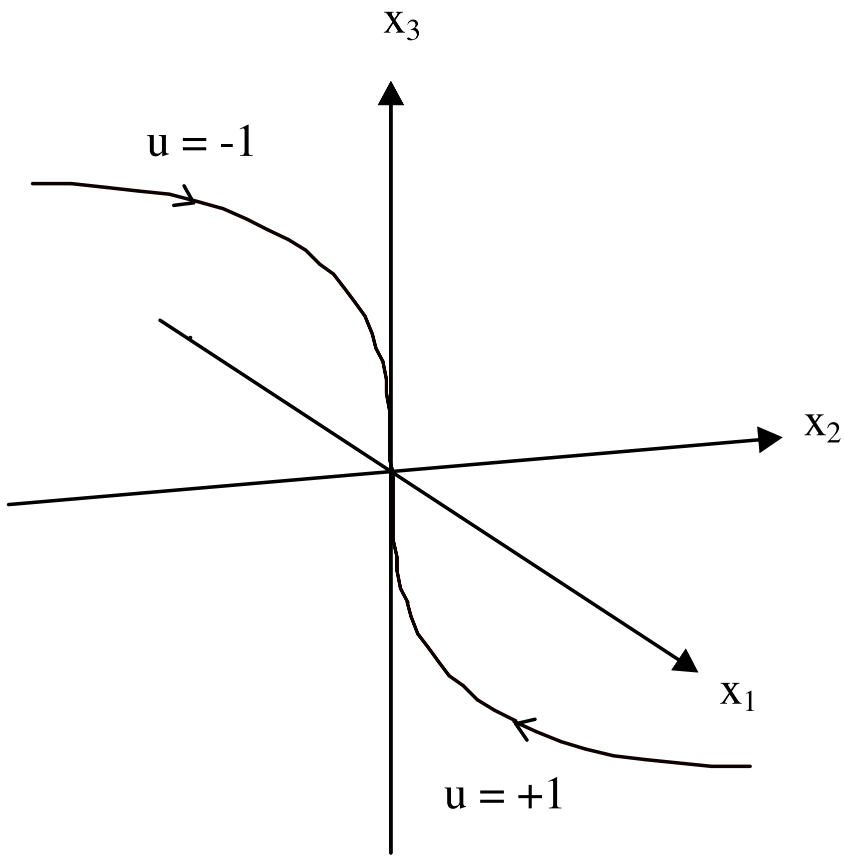

Figure 4

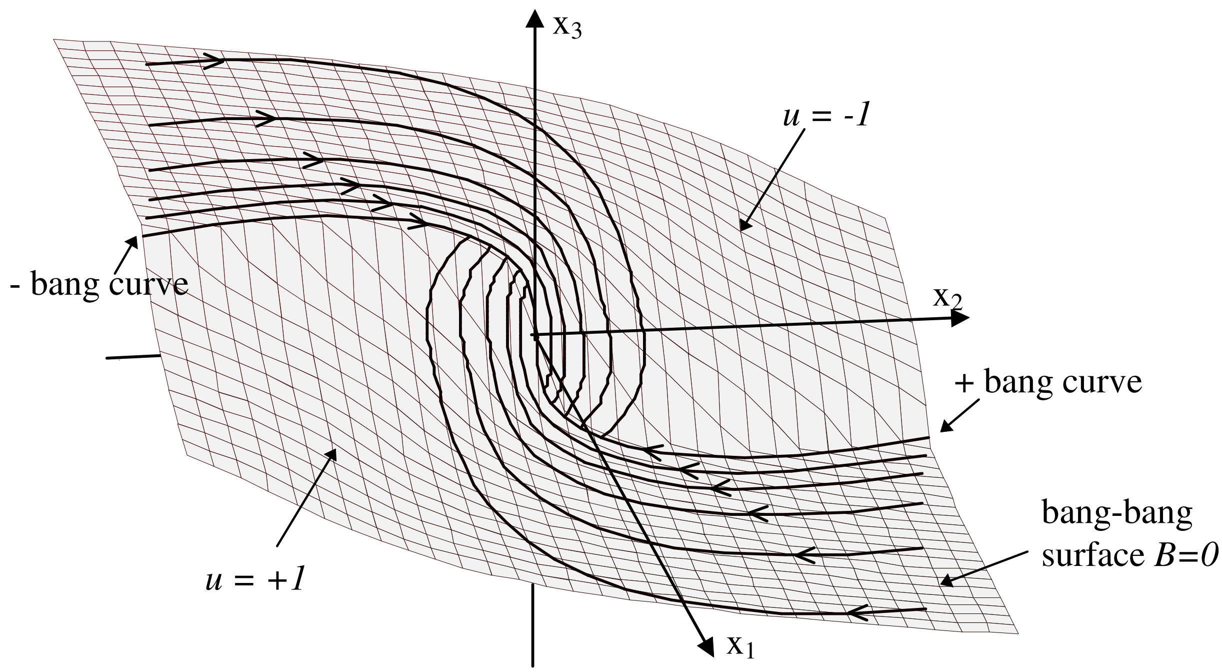

Figure 5

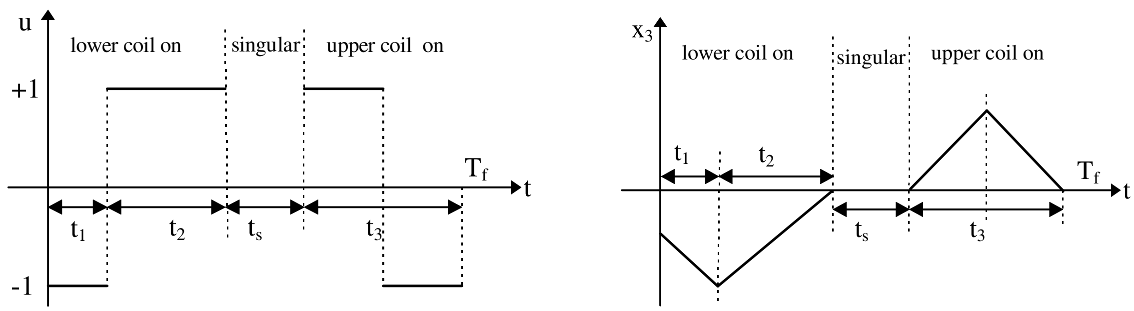

u
lower coil on
singular
upper coil on
+1
-1
T_f
t
t_1
t_2
t_s
t_3
x_3
lower coil on
singular
upper coil on
t_1
t_2
T_f
t
t_s
t_3

Figure 6

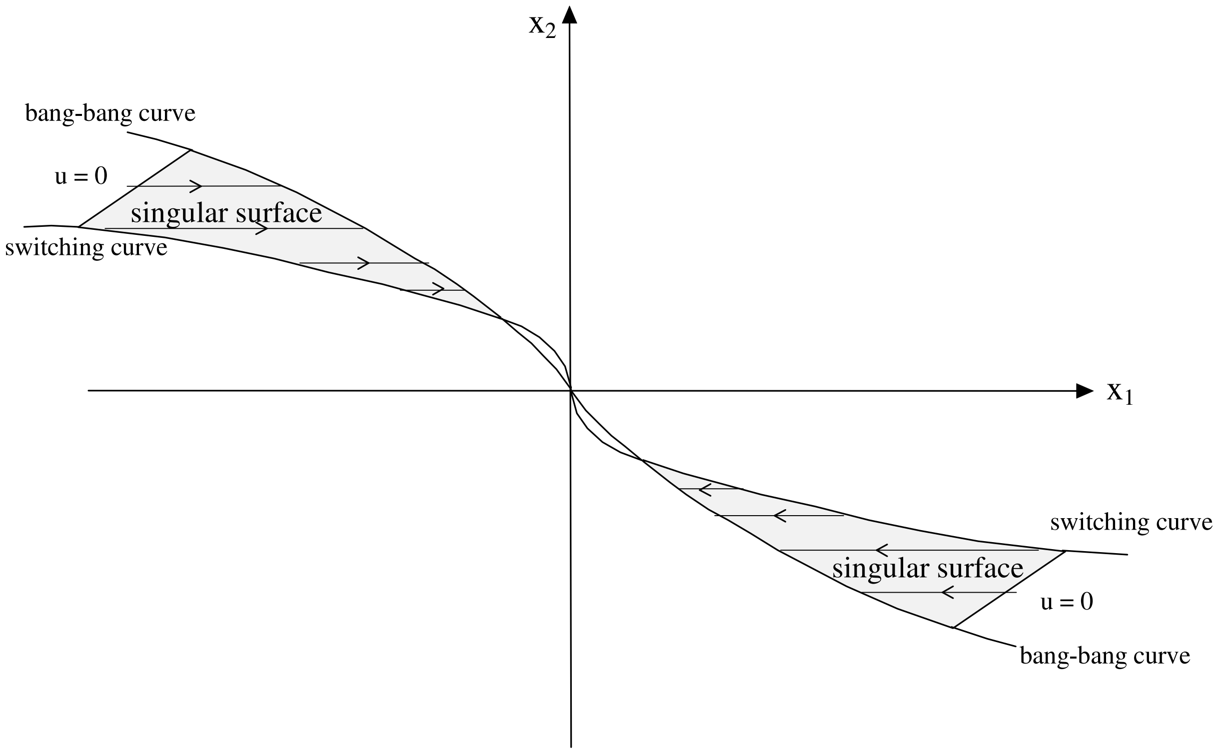

x_2
x_1
bang-bang curve
u = 0
singular surface
switching curve
switching curve
singular surface
u = 0
bang-bang curve

Figure 7

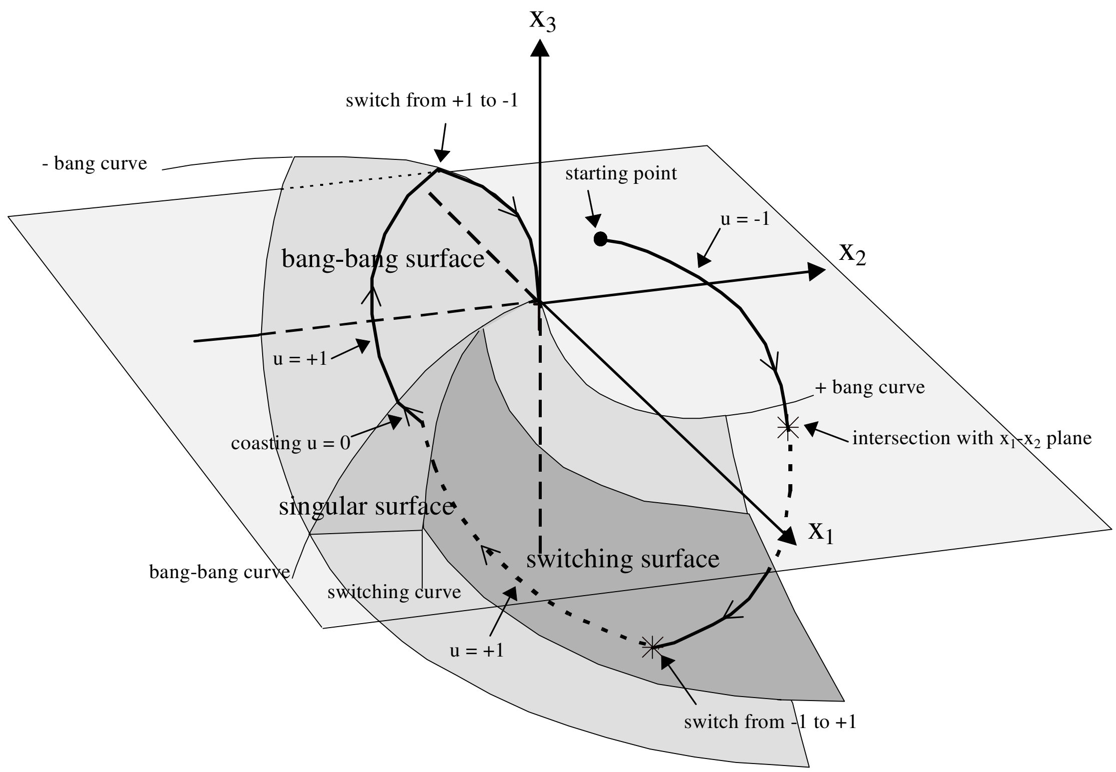

x_3
switch from +1 to -1
- bang curve
starting point
u = -1
x_2
bang-bang surface
u = +1
+ bang curve
intersection with x_1-x_2 plane
coasting u = 0
singular surface
x_1
switching surface
bang-bang curve
switching curve
u = +1
switch from -1 to +1

Figure 8a

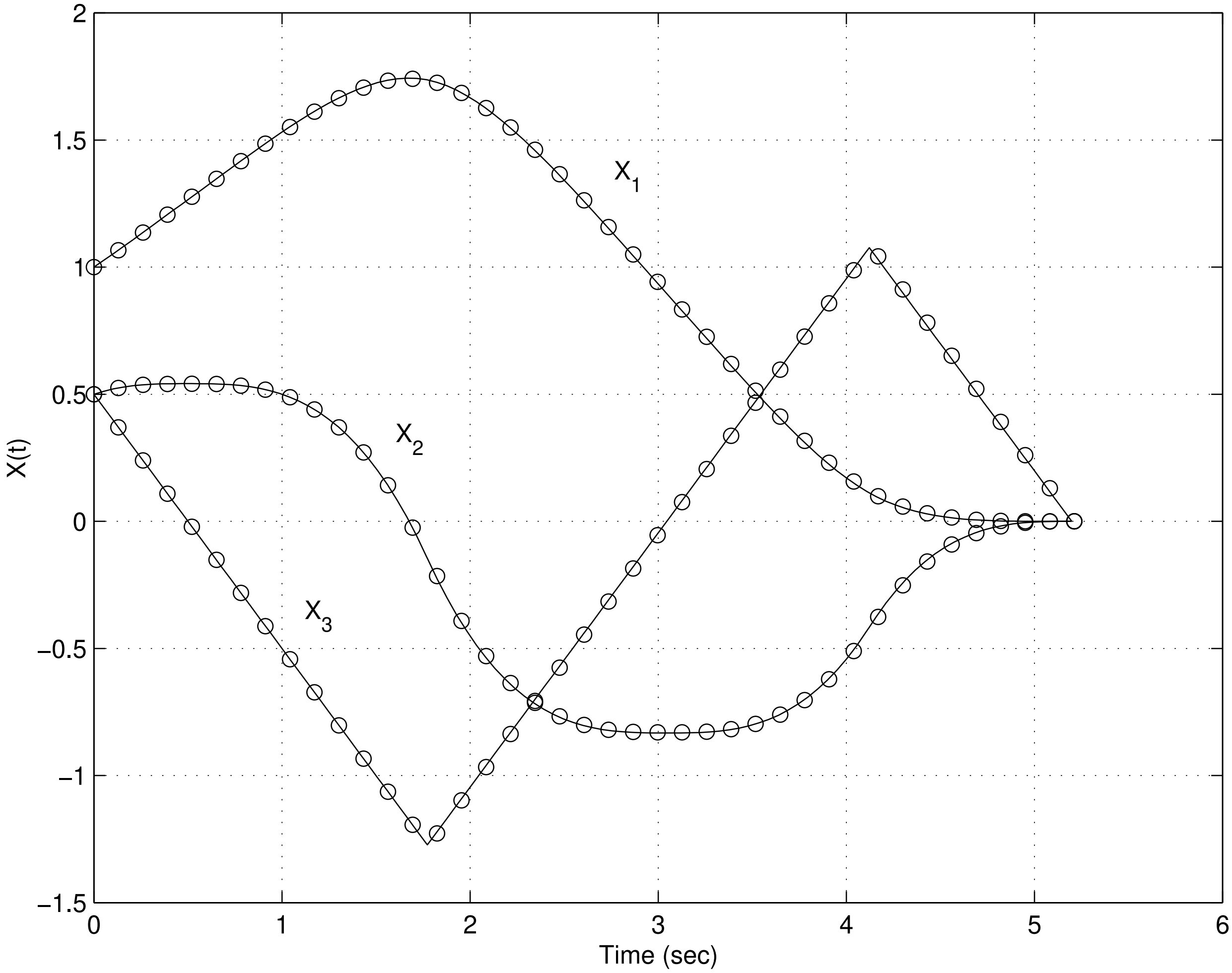

Figure 8b

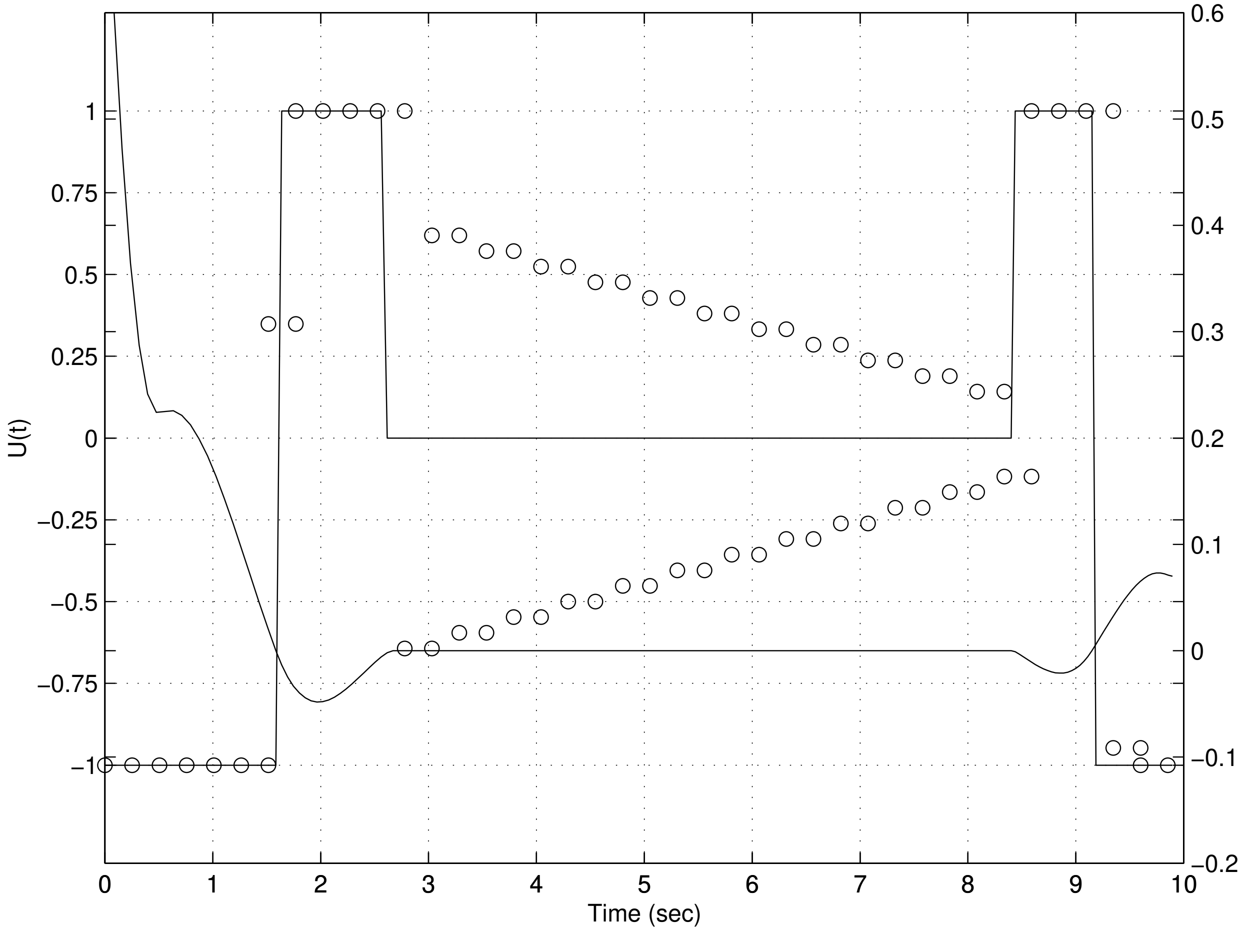
U(t)
1
0.75
0.5
0.25
0
−0.25
−0.5
−0.75
−1
0.6
0.5
0.4
0.3
0.2
0.1
0
−0.1
−0.2
0 1 2 3 4 5 6 7 8 9 10
Time (sec)

Figure 9a

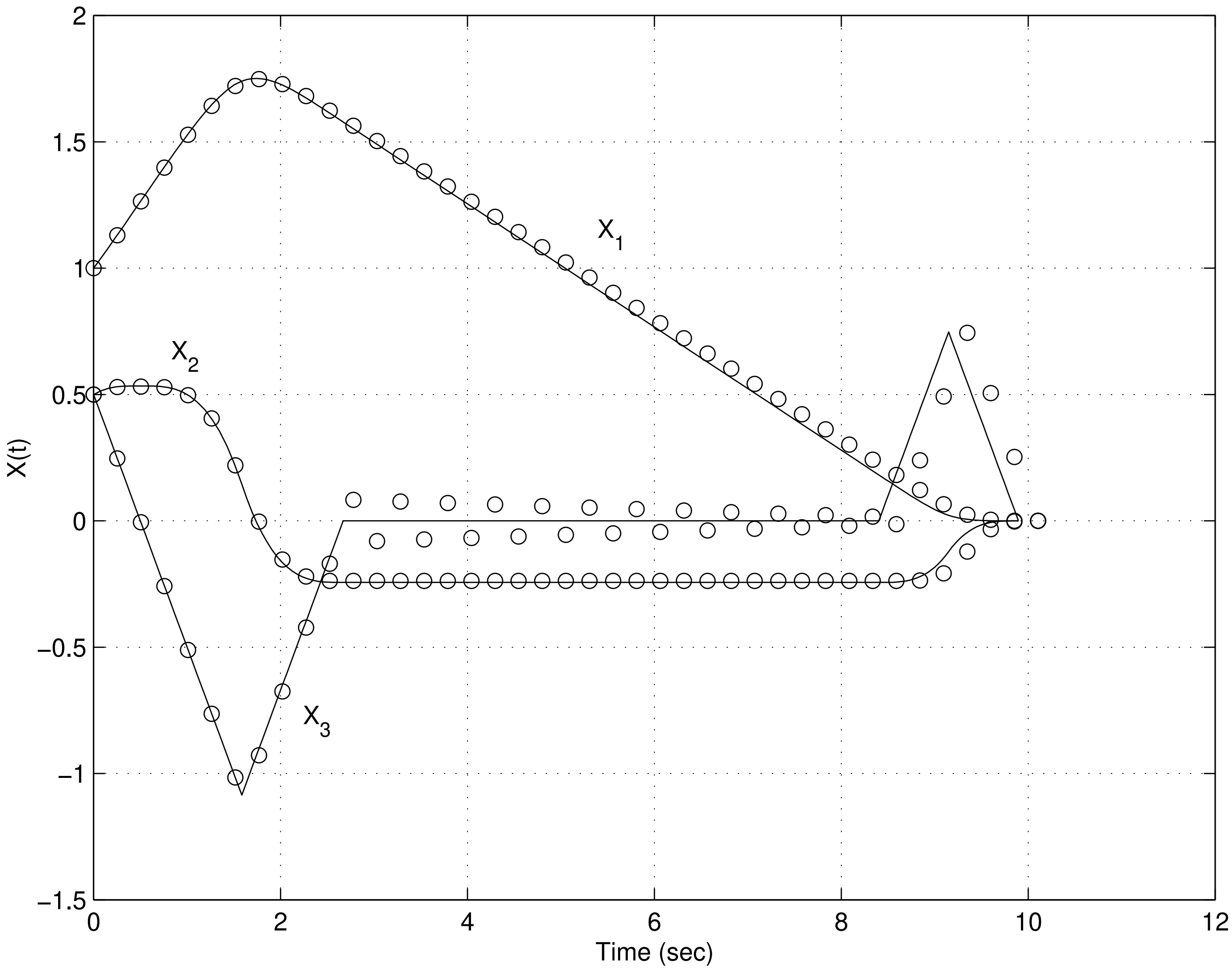

Figure 9b

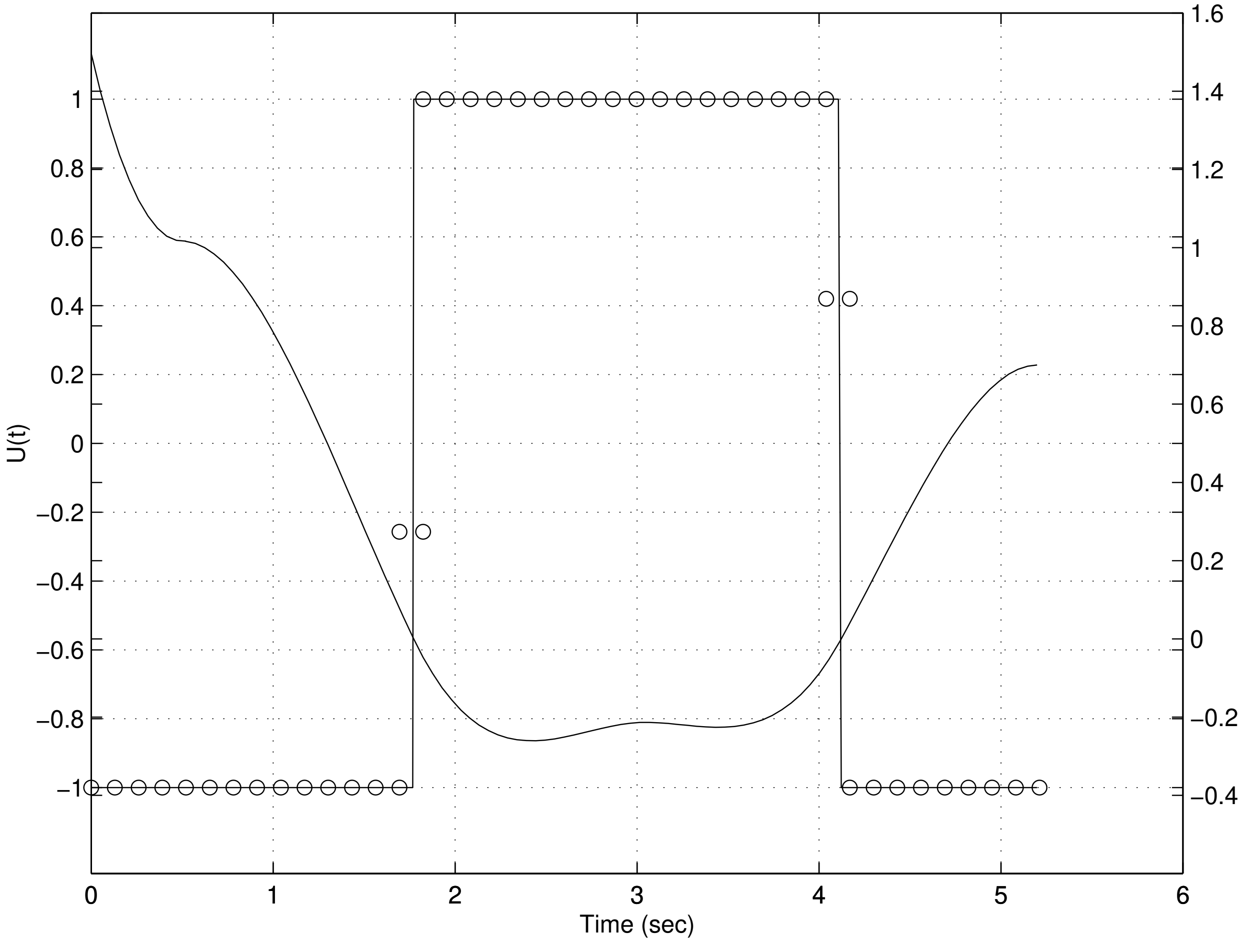

U(t)
Time (sec)
0
1
2
3
4
5
6
1
0.8
0.6
0.4
0.2
0
−0.2
−0.4
−0.6
−0.8
−1
1.6
1.4
1.2
1
0.8
0.6
0.4
0.2
0
−0.2
−0.4

List of Figures